Dynamic Structure Formation at the Fronts of Volatile Liquid Drops

Y. Gotkis,[1] I. Ivanov,[2] N. Murisic,[3] and L. Kondic[3]
[1]KLA-Tencor Corporation, San Jose, California 95134, USA
[2]Blue29, Sunnyvale, California 94085, USA
[3]Department of Mathematical Sciences, New Jersey Institute of Technology, Newark, New Jersey 07102, USA
(Received 20 July 2006; published 30 October 2006)

We report on instabilities during the spreading of volatile liquids, with emphasis on the novel instability observed when isopropyl alcohol is deposited on a monocrystalline Si wafer. This instability is characterized by emission of drops ahead of the expanding front, with each drop followed by smaller, satellite droplets, forming the structures which we nickname ''octopi'' due to their appearance. A less volatile liquid, or a substrate of larger heat conductivity, suppresses this instability. We formulate a theoretical model that reproduces the main features of the experiment.

DOI: 10.1103/PhysRevLett.97.186101 PACS numbers: 68.03.Fg, 47.20.Dr, 47.50.Gj, 68.15.+e

The phenomenon of drying liquid thin films has recently attracted significant attention from the scientific and engineering communities. One reason for this interest is the fact that advanced semiconductor technologies are very sensitive to the residues, called watermarks, on the semiconductor wafer surfaces which occur when microdrops of high purity deionized water (DIW) are left to dry [1]. Although the formation of watermarks has been analyzed [2,3], their origin is still not completely clear, in particular, in the settings relevant to applications [4]. Additional features, such as the formation of dry spots resulting from film integrity breakage, are of considerable relevance as well. These features are often connected to various hydrodynamic instabilities which occur in evaporative films [3]. One novel type of instability, which may help us learn about the basic physical processes that govern the dynamics, is the main subject of this Letter.

Figure 1 illustrates the experimental observation on which we concentrate (see also associated video clips [5]). As a (mother) drop of isopropyl alcohol (IPA) is deposited on a surface, it expands and ejects fluid ahead of its front. This material nucleates into smaller (head) drops all around its perimeter, followed by smaller (satellite) drops which travel along the paths already traversed by the head drops. These structures (nicknamed ''octopi'' since the head drop appears as an octopus body and streams of satellite drops as several tentacle arms) occur just for a particular liquid-solid configuration and belong in turn to a wider family of patterns which may form in evaporative systems. We note that the octopi appear to be separated from the mother drop, while most of the previously observed patterns, such as festoons [6], fingers [3,7], or the drops in electric fields [8], were connected to the main fluid body. We also note that the instabilities reported here are clearly very different from the droplet formation by recondensation [9], and they occur for pure liquids, in contrast to the instabilities in the presence of surfactants [10,11]. The features such as complexity of the octopi and the fact that they appear to function as a single object while actually consisting of multiple but disconnected parts makes these structures unique.

In this work we describe experimental techniques used and present a model which gives a basic understanding of the instability mechanism in a simplified flow geometry. We show that an explanation of the instability mechanism requires inclusion of a large number of effects, including evaporation and thermal effects in all three phases (gas, liquid, and solid), in addition to modeling the motion of liquid fronts. We are not aware of any previous work that includes all the relevant effects.

The experiments are performed by depositing drops of IPA or IPA-deionized water (DIW) mixtures of a typical size of 30–50 mm^3 on wafers of monocrystalline Si (thick-

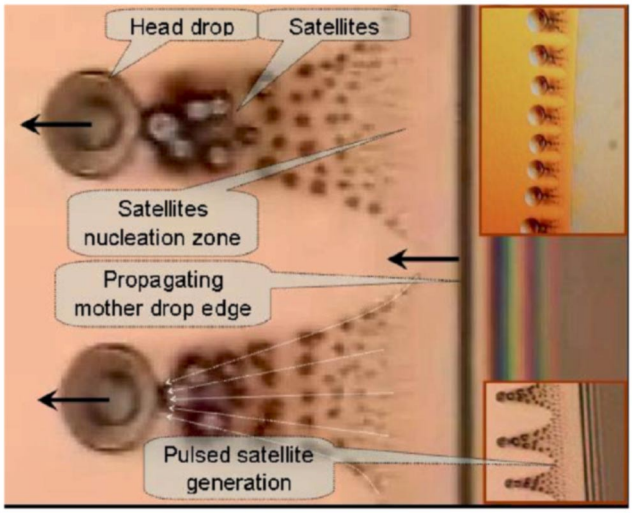

FIG. 1 (color online). Formation of octopi during spreading of IPA drop on a Si surface. The bands on the right-hand side are due to Newton interference fringes. White arrows indicate the path of the satellites. On the scale shown ($\approx 200 \times 300$ μm) the azimuthal curvature of the (mother) drop is invisible. The insets show uniformity of the octopi (top inset) and synchronous pulselike emission of satellites (bottom inset).

ness 0.75 mm), bare or coated with copper film. All materials used are of semiconductor grade quality. The solid surfaces were treated by chemical-mechanical polishing, producing surface roughness (rms) of 0.5 nm for Si and 1 nm for Cu films. The measurements were performed under clean room conditions at 25 °C, using a Sony AL 100M microscope with a video camera. We have verified that possible heating of the surface by the microscope illuminator does not influence the results.

Figure 1 shows octopi formation, which occurs (only) for one of the four configurations considered (two liquid and two solid types), and that is an IPA drop on a Si surface. The octopilike patterns are robust and have occurred consistently in all experiments involving this liquid-solid combination. During the initial period after deposition, the drop front spreads, the drop quickly reaches the thickness of few fractions of a millimeter, and the fluid is ejected through the front, forming the head drops spaced regularly around the perimeter. Behind the head drops, satellites propagate, which are either emitted by the front itself or nucleated at some distance ahead. These satellites increase in size by merging and/or picking up some material from the prewetted trail left by the head drops. This prewetted trail leads to faster motion of the satellites and to their focusing towards the head drops. One simple explanation of both effects is that the satellite motion is enhanced on this prewetted trail [12]. Eventually, the satellites catch up with the head drops and merge, returning the mass and kinetic energy lost to the interaction with the substrate, formation of the prewetted trail, and evaporation, leading to the perhaps surprising fact that the head drops move with exactly the same speed as the drop front itself. Therefore, the structures shown in Fig. 1 are steady in the moving frame translating with the speed of the front (see also [5]). We note that the satellites are often generated in temporal pulses during which a radial wave of satellites is emitted all around the perimeter (viz., Fig. 1, lower inset). A possible explanation of this effect can be reached by considering IPA-DIW mixture, discussed below.

So far we have focused on the first, expanding part of the drop evolution. This part, which lasts $\approx$40–50 s, is followed by the contraction phase ($\approx$5–7 s) during which the remaining film quickly retracts toward the center, evaporating and disintegrating into a multitude of swiftly evaporating microdroplets. The head drops move forward for a while longer, and then stop. The fact that the octopi do not retreat together with the film edge additionally shows that there is no physical link between the octopi and the mother drop.

Spreading of IPA-DIW drops also leads to instabilities, but of different types. Figure 2 shows that in the case of 1:1 mixture, the drop front develops unsteady patterns (cells). At some stage of evolution, the individual cells start to converge and form a peripheral ridge (viz., the bottom row of Fig. 2). This ridge propagates or collapses toward the center of the drop and then rebounds inducing global oscillatory motion [13]. We expect that a similar effect is

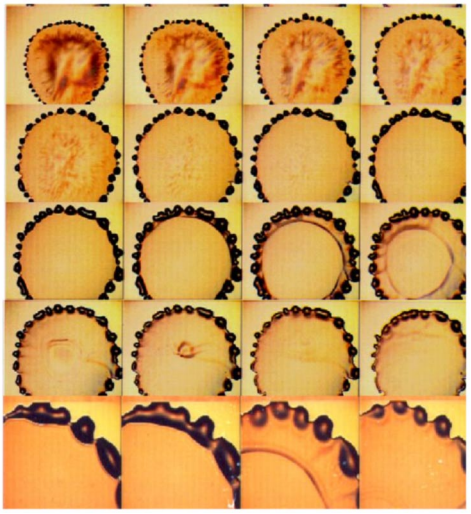

FIG. 2 (color online). Spreading of 1:1 mix of DIW/IPA. Drop size is approximately 5 mm. The darker color indicates increased fluid thickness. Time progresses left to right and top to bottom, with the interval between the images $\approx$ 1.5 s. The bottom row illustrates the merge of individual cells just prior to wave generation (close to image 10). Note formation of radial ridges during early stages of instability development.

responsible for global synchronous emission of satellites for pure IPA drop. We note that propagation of the waves across the drop surface may lead to a variety of effects, including formation of dry spots. We will discuss these effects, as well as spreading on Cu coated substrates, in more detail in future works.

We devote the rest of this Letter to formulating a mathematical model that explains some basic features of the experimental results. For brevity we concentrate only on the most novel feature of the experiments, and that is formation of the head drops, i.e., the instability mechanism which leads to detachment or ejection of the film material through the front of the mother drop. Future works will discuss other relevant questions, such as distance between octopi, formation of satellites, etc. However, for the purpose of understanding in a qualitative manner the basic process leading to ejection of head drops, it is sufficient to consider a simplified 2D geometry (cross section of a drop). In formulating an appropriate model, we are governed by the fact that the octopi occur only in the case of IPA (strong evaporation, low thermal conductivity) spreading on a surface of low thermal conductivity. This suggests that we need to include at least evaporation and the heat conduction in the liquid and solid, in addition to other obvious physical mechanisms.

The starting point is the Navier-Stokes equations in two dimensions for incompressible viscous fluid, accompanied by the energy equations for the liquid and solid. We consider a physical setup with $h(x, t)$ as film thickness and x, z as the coordinates along and normal to the substrate; the liquid-solid interface is at $z = 0$ and the liquid-vapor interface is at $z = h(x, t)$. The boundary conditions include the

following: fixed solid temperature at $z = -d_s$ (the bottom of the solid layer); no slip and matching temperatures and heat fluxes at $z = 0$; mass balance, energy balance, and normal and shear stress balance at $z = h(x, t)$.

The main building blocks of our model are as follows: (i) The spreading mother drop is characterized by a small aspect ratio so that lubrication approximation is appropriate. (ii) Marangoni forces seem to be crucial, so we include dependence of surface tension on temperature $\sigma(T) = \sigma_0 - \gamma(T - T_0)$, where $\sigma_0 = \sigma(T_0)$ and T_0 is the room temperature. (iii) The experiments are performed in an open atmosphere undersaturated by vapor, justifying the use of a one-sided model for evaporation [14–16]. (iv) Thermal and vapor recoil effects are included [14,15]. (v) Wetting properties of the fluids are considered using a disjoining pressure model [17] corresponding to the formation of a stable precursor film. Inclusion of the considered physical mechanisms leads to the following nondimensional equation for the liquid height h as a function of the in-plane coordinate x (see, e.g., [15]):

$$\frac{\partial h}{\partial t} + \frac{E}{h + \mathcal{K} + \mathcal{W}} + S(h^3 h_{xxx})_x + \left[\left(\frac{E^2 h^3}{D(h + \mathcal{K} + \mathcal{W})^3} + \frac{\mathcal{K} M h^2}{P(h + \mathcal{K} + \mathcal{W})^2}\right) h_x\right]_x + A\{h^3[(b/h)^3 - (b/h)^2]_x\}_x + B(h^3 h_x)_x = 0. \quad (1)$$

Here, the terms are due to viscous dissipation, evaporation, capillarity (first row), vapor recoil, thermal Marangoni effects (second row), disjoining pressure, and gravity, respectively. We use the following scales (all parameters are for liquid unless otherwise noted): the length scale is typical drop thickness, $d_0 = 0.5$ mm; d_0^2/ν, ν/d_0, $\rho\nu^2/d_0^2$, and $\Delta T = T_0 - T_{\text{sat}}$ are the scales for time, velocity, pressure, and temperature; here ν and ρ are viscosity and density, and T_{sat} is the saturation temperature at given vapor pressure. The parameters are as follows (using the notation in [14]): evaporation number $E = k\Delta T/(\rho\nu L)$, $\mathcal{K} = (2\pi R_g)^{1/2} k T_{\text{sat}}^{3/2}/(\alpha d_0 \rho_v L^2)$, $\mathcal{W} = d_s k/(d_0 k_s)$, $S = \sigma_0 d_0/(3\rho\nu^2)$, Marangoni number $M = \gamma\Delta T d_0/(2\rho\nu\kappa)$, and Prandtl number $P = \nu/\kappa$; $D = 3\rho_v/(2\rho)$, $B = -d_0^3\rho^2 g/(3\mu^2)$, and disjoining pressure coefficient $A = s d_0\rho/(3\mu^2 N b)$, where k is thermal conductivity, L is latent heat of vaporization, α is the accommodation coefficient, ρ_v is vapor density, and R_g is the ratio of the gas constant and molar mass; d_s and k_s are the thickness and thermal conductivity of solid; $\gamma = -d\sigma/dT$, $\kappa = k/(c_p\rho)$, where c_p is heat capacity; μ is dynamic viscosity; $b = 0.01$ is the precursor film thickness, $s = \sigma_0(1 - \cos\theta)$, and $N = (n - m)/[(n - 1)(m - 1)]$ [we use $(n, m) = (3, 2)$ [17]]. θ is equilibrium contact angle (see also [9,17]). We note that, while lubrication approximation is strictly valid only for $\theta \approx 0$, it is known that it produces accurate results even for relatively large θ's (see, e.g., [18]). Table I lists the most important parameters; here we use the values for pure IPA and DIW.

The value of α, which is the probability of phase change for a liquid molecule at the interface, requires a comment. Since only the range of values $[0, 1]$ is known [14,20], we estimate it using experimentally measured dry out times, and the expression for the mass flux between the liquid and the vapor phase $j_0 = \alpha\rho_v[(RT_i)/(2\pi)]^{1/2}$ [20]. Here the interface temperature T_i is obtained using temperature drop at the IPA-vapor interface of 15 K, which follows from a simple model that assumes that liquid temperature obeys the Laplace equation.

An estimate of time scales relevant to heat transport gives useful insight; here we concentrate on IPA on Si. First, we note that calculating the evaporation rate requires an estimate of the saturation temperature T_{sat}; for this purpose we use the Clausius-Clapeyron relation [20]. The evaporation time scale is [14] $d_0^2\rho L/(k\Delta T) \approx 30$ s, comparable to the dry out time observed in our experiments. The time scale for vapor diffusion is d_0^2/D_m ($\approx 10^{-5}$ s), where mass diffusion coefficient D_m is estimated from Fick's law; such a short time scale enhances evaporation. Next, liquid heat conduction time scale d_0^2/κ is ≈ 0.03 s, while for the solid it is d_s^2/κ_s (κ_s is thermal diffusivity of the solid), which is close to 600 s. The disparity of the time scales leads to strong temperature gradients and the associated Marangoni effect. Similar estimates for other liquid-solid combinations show that a weaker Marangoni effect is expected due to increased heat conductivity of DIW and/or Cu.

We proceed in two stages. First, we consider briefly linear stability analysis (LSA) of a flat infinite film, exploring whether instability can be expected for the relevant physical parameters in this simplified geometry. Then, we report results of fully nonlinear simulations of the Eq. (1) for the initial condition resembling the experiment.

Figure 3 shows LSA results for four considered configurations, performed by perturbing a flat film of the thickness d_0 by a harmonic perturbation of a given wavelength λ. We find that the flow is unstable for wave numbers $k < k_c$. For

TABLE I. Table of parameter values for IPA and DIW [19].

Parameter	IPA	DIW
T_{sat}[K]	247	250
ρ_v[kg/m^3]	2.0	0.9
ρ[kg/m^3]	785	998
γ[N/(K m)]	2.5×10^{-4}	1.8×10^{-4}
α	3.3×10^{-5}	10^{-5}
θ_{Si}[deg]	20	5
θ_{Cu}[deg]	25	10
σ_0[N/m]	2.1×10^{-2}	7.2×10^{-2}
L[J/kg]	7.9×10^5	2.44×10^6
R_g[J/(kg K)]	138.35	461.92
μ[kg/(ms)]	2.04×10^{-3}	0.9×10^{-3}
k[W/(K m)]	0.135	0.605
k_s[W/(K m)] (Si)	1.35	1.35
k_s[W/(K m)] (Cu)	390	390

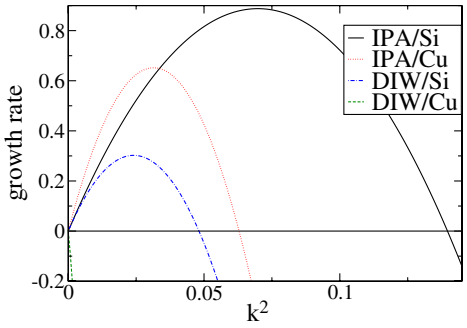

FIG. 3 (color online). Results of LSA for a uniform fluid film.

a Si substrate, we get the critical $\lambda_c = 2\pi/k_c \approx 8.4$ mm for IPA, and a larger value $\lambda_c \approx 1.43$ cm for DIW. On a Cu substrate, $\lambda_c \approx 1.25$ cm for IPA; DIW on Cu is stable. Although the values of λ_c's are larger than the patterns occurring in the experiments, the results are encouraging since they show that the resulting λ_c's are much smaller for IPA compared to DIW, and the corresponding growth rates are larger. Also, LSA suggests that instability is more likely for IPA on Si than on Cu, again in agreement with the experiments.

Figure 4 shows the drop shapes as a function of time resulting from fully nonlinear simulations of Eq. (1), performed using a finite difference method (see, e.g., [21]). An initial condition (not shown) for the four cases is a cylindrical cap. We see that only IPA on Si leads to instabilities in front of the drop, in direct agreement with the experiment. We note that there are no fitting parameters in the model and that all parameters are appropriate for the considered fluids and solids. Therefore we conclude that the proposed model can be successfully used to explain the basic instability mechanism observed in the experiments. Note that "switching off" of evaporation completely removes the instability, showing its crucial role. Much more detailed computational results including quantitative comparison between the experiments and simulations will be presented elsewhere.

In this Letter we have presented a novel fluid instability resulting in a complex structure formation developing at

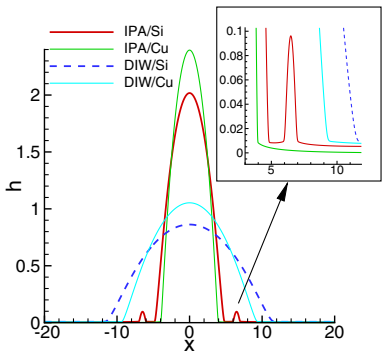

FIG. 4 (color online). Fluid profiles at $t = 1$. The inset zooms in on the region of instability for the IPA/Si case.

the fronts of volatile liquid drops. These structures, occurring only for spreading of highly volatile liquid on a substrate characterized by small thermal conductivity and resulting from an interplay of the heat and mass transfer between solid, liquid, and gas, show that all three phases are important in reaching an understanding of the dynamics of volatile fluids. Other related effects, such as contact line instabilities, formation of dry spots, particle transport and deposition, among others, have been observed and will be considered in future works.

The authors would like to thank Burt Tilley and Thomas Witelski for useful comments.

[1] International Technology Roadmap for Semiconductors, http://public.itrs.net/.
[2] R. Deegan *et al.*, Nature (London) **389**, 827 (1997).
[3] M. Gonuguntla and A. Sharma, Langmuir **20**, 3456 (2004).
[4] J. Prasad, Semicond. Int. **27**, 61 (2004).
[5] See EPAPS Document No. E-PRLTAO-97-029645 for movies of selected experiments. For more information on EPAPS, see http://www.aip.org/pubservs/epaps.html.
[6] C. Redon *et al.*, J. Phys. II **2**, 1671 (1992).
[7] M. Cachile, O. Benichou, and A. Cazabat, Langmuir **18**, 7985 (2002).
[8] F. Mugele and S. Herminghaus, Appl. Phys. Lett. **81**, 2303 (2002).
[9] C. Poulard, O. Benichou, and A. Cazabat, Langmuir **19**, 8828 (2003).
[10] M. Cachile *et al.*, Colloids Surf. A **159**, 47 (1999).
[11] O. K. Matar and S. M. Troian, Phys. Fluids **10**, 1234 (1998).
[12] L. Kondic and J. Diez, Phys. Rev. E **65**, 045301 (2002).
[13] P. Kavehpour, B. Ovryn, and G. McKinley, Colloids Surf. A **206**, 409 (2002).
[14] J. P. Burelbach, S. G. Bankoff, and S. H. Davis, J. Fluid Mech. **195**, 463 (1988).
[15] A. Oron, S. H. Davis, and S. G. Bankoff, Rev. Mod. Phys. **69**, 931 (1997).
[16] V. Ajaev, J. Fluid Mech. **528**, 279 (2005); H. Hu and R. Larson, Langmuir **21**, 3963 (2005); E. Sultan, A. Boudaoud, and M. Ben Amar, J. Fluid Mech. **543**, 183 (2005).
[17] L. W. Schwartz *et al.*, J. Colloid Interface Sci. **234**, 363 (2001).
[18] A. Münch and B. Wagner, Physica (Amsterdam) **209D**, 178 (2005).
[19] *Handbook of Chemistry and Physics*, edited by D. Lide (CRC Press, New York, 1997), 78th ed.; International Programme on Chemical Safety (IPCS), http://www.inchem.org.
[20] E. Kennard, *Kinetic Theory of Gases with an Introduction to Statistical Mechanics* (McGraw-Hill, New York, 1938); *A Theoretical Study of Interphase Mass Transfer* (Columbia University Press, New York, 1953); T. Ishiyama, T. Yano, and S. Fujikawa, Phys. Rev. Lett. **95**, 084504 (2005).
[21] J. Diez and L. Kondic, J. Comput. Phys. **183**, 274 (2002).